Blocked populations in ring-shaped optical lattices

M. Nigro, P. Capuzzi, and D. M. Jezek
Universidad de Buenos Aires, Facultad de Ciencias Exactas y Naturales, Departamento de Física, Buenos Aires, Argentina and IFIBA, CONICET-UBA, Pabellón 1, Ciudad Universitaria, 1428 Buenos Aires, Argentina

(Received 25 April 2018; revised manuscript received 26 August 2018; published 19 December 2018)

We study a special dynamical regime of a Bose-Einstein condensate in a ring-shaped lattice where the populations in each site remain constant during the time evolution. The states in this regime are characterized by equal occupation numbers in alternate wells and nontrivial phases, while the phase differences between neighboring sites evolve in time yielding persistent currents that oscillate around the lattice. We show that the velocity circulation around the ring lattice alternates between two values determined by the number of wells and with a specific time period that is only driven by the on-site interaction energy parameter. In contrast to the self-trapping regime present in optical lattices, the occupation number at each site does not show any oscillation and the particle imbalance does not possess a lower bound for the phenomenon to occur. These findings are predicted with a multimode model and confirmed by full three-dimensional Gross-Pitaevskii simulations using an effective on-site interaction energy parameter.

DOI: 10.1103/PhysRevA.98.063622

I. INTRODUCTION

The self-trapping phenomenon has been extensively studied in double-well systems by means of a two-mode model [1–8], and was experimentally observed by Albiez *et al.* [9–11]. In this regime the population in one site remains higher than the one in the other well over all the evolution. This imbalance of particles performs oscillations around the nonvanishing mean value, whereas the phase difference between the sites exhibits a running phase behavior. Theoretical studies of this phenomenon have been also carried out by several authors in extended regular lattices [12–15]. More recently, the study of self-trapping has also been addressed in ring-shaped optical lattices [16–18]. Such works treat three- and four-well systems. In Refs. [16,17] the dynamics was investigated through a multimode (M) model that utilized *ad hoc* values for the hopping and on-site energy parameters. However, in Ref. [18], such parameters were extracted from a mean-field approach using three-dimensional localized "Wannier-like" (WL) on-site functions and including an effective on-site interaction energy parameter [19,20]. For large filling numbers, the inclusion of such a realistic interaction parameter has been shown to be crucial for the accurate description of the dynamics, yielding a sizable change on the time periods with respect to those obtained by the standard model. In contrast, for filling number around unity, mean-field approaches are not applicable and hence other microscopic methods have to be used [21,22]. In Ref. [23], it was demonstrated that an effective interaction can also be extracted from the Bogoliubov excitations in the case of the Josephson regime. A systematic study of the self-trapping regime and the crossover to the Josephson oscillations in four-well systems including nonsymmetric configurations was developed in Ref. [18]. It is worthwhile to notice that the dynamics in multiple-well condensates constitutes a promising area provided that successful efforts have been performed to experimentally construct ring-shaped optical lattices [24].

In this work we demonstrate theoretically the existence of a dynamical regime that exhibits a novel behavior. If the number of wells of the lattice is a multiple of 4, there exists a family of nonstationary states with constant site populations and special nontrivial phases. These states could be regarded as a special variation of a ST regime where, in contrast to that observed in two- and multiple-well condensates [1,2,7,18], the population imbalance between neighboring sites can be arbitrarily low and does not exhibit any oscillation in time. For such states the M model order parameter can be expressed as a linear combination of particular degenerate Gross-Pitaevskii (GP) stationary states. However, due to the nonlinear nature of the GP equation, the states are nonstationary. The dynamics of these states is governed only by the on-site interaction energy parameter. We explicitly show that the angular momentum exhibits a simple oscillating behavior and that the velocity circulation around the ring alternates periodically between values $-N_c/4$ and $N_c/4$, N_c being the number of weakly linked condensates. A goal of this work is to obtain an analytical expression for such a time period which involves only the imbalance and the effective interaction parameter. By comparing the evolution of the phase differences obtained through GP simulations for a four-well system and with the M model, we can establish the accuracy of such a parameter. The existence of these states is confirmed numerically by means of full three-dimensional GP simulations showing a perfect accordance to the M model predictions for several population imbalances. Furthermore, a Floquet stability analysis confirms that for the imbalances studied here the dynamics turns out to be regular.

The paper is organized as follows. In Sec. II we briefly review the main concepts of the multimode model. In particular, we rewrite the equations of motion which include an effective on-site interaction parameter [18] and we outline the construction of the localized states in terms of the GP stationary ones. In Sec. III we describe the specific four-well system used in

the numerical simulations. Section IV is devoted to studying the properties of these states with blocked occupation numbers. As a first step we introduce a continuous family of states corresponding to fixed points of the M model in the phase diagram defined by the populations and phase differences. On the other hand, we demonstrate that they turn out to be quasistationary solutions of the GP equation. Such states are defined with a particular combination of phases which give rise to the nonstationary blocked-occupation-number (BON) states. Second, we show that these BON states describe closed orbits in the phase diagram whose time period is solely determined by the on-site interaction energy. By performing GP numerical simulations with a four-well potential we analyze the hidden dynamics which includes variations of density in the interwell regions, oscillations of the velocity field circulation, and an active vortex dynamics. We end this section with a study of the Floquet stability of the BON states and a proposed experimental test. In Sec. V we show how to generalize the previous results for systems with larger numbers of sites. To conclude, a summary of our work is presented in Sec. VI and the definition of the parameters employed in the equations of motion are gathered in the Appendix.

II. MULTIMODE MODEL

The equations of motion of the multimode model have been previously studied both for multiple-well systems in general [20,25] and also in the case of a four-well system [16,18]. Here, we only review their main ingredients, focusing on the definition of their localized states extracted from the stationary solutions of the GP equations.

A. Multimode model equations of motion including interaction-driven corrections

Using the multimode model order parameter,

$$\psi_M(t,\mathbf{r}) = \sum_k b_k(t)\, w_k(r,\theta,z), \tag{1}$$

written in terms of three-dimensional WL functions localized at the k site, $w_k(\mathbf{r})$ [18], one obtains the equations of motion for the time-dependent coefficients $b_k(t) = e^{i\phi_k}\,|b_k|$ by replacing the order parameter in the time-dependent GP equation. The $2N_c$ real equations, written in terms of the populations $n_k = |b_k|^2 = N_k/N$ and phase differences $\varphi_k = \phi_k - \phi_{k-1}$ including effective on-site interaction corrections [18], are

$$\begin{aligned}\hbar\frac{dn_k}{dt} &= -2J[\sqrt{n_k\,n_{k+1}}\,\sin\varphi_{k+1} - \sqrt{n_k\,n_{k-1}}\,\sin\varphi_k]\\ &\quad - 2F[\sqrt{n_k\,n_{k+1}}(n_k+n_{k+1})\,\sin\varphi_{k+1}\\ &\quad - \sqrt{n_k\,n_{k-1}}(n_k+n_{k-1})\,\sin\varphi_k],\end{aligned} \tag{2}$$

$$\begin{aligned}\hbar\frac{d\varphi_k}{dt} &= (n_{k-1}-n_k)NU_{\rm eff}\\ &\quad - \alpha(n_{k-1}-n_k)NU[N_c(n_{k-1}+n_k)-2]\\ &\quad - J\left[\left(\sqrt{\frac{n_k}{n_{k-1}}} - \sqrt{\frac{n_{k-1}}{n_k}}\right)\cos\varphi_k\right.\\ &\quad \left. + \sqrt{\frac{n_{k-2}}{n_{k-1}}}\,\cos\varphi_{k-1} - \sqrt{\frac{n_{k+1}}{n_k}}\,\cos\varphi_{k+1}\right]\\ &\quad - F\left[\left(n_k\sqrt{\frac{n_k}{n_{k-1}}} - n_{k-1}\sqrt{\frac{n_{k-1}}{n_k}}\right)\cos\varphi_k\right.\\ &\quad + \left(3\sqrt{n_{k-2}\,n_{k-1}} + n_{k-2}\sqrt{\frac{n_{k-2}}{n_{k-1}}}\right)\cos\varphi_{k-1}\\ &\quad \left. - \left(3\sqrt{n_{k+1}\,n_k} + n_{k+1}\sqrt{\frac{n_{k+1}}{n_k}}\right)\cos\varphi_{k+1}\right],\end{aligned} \tag{3}$$

where $U_{\rm eff} = f_{3D}U$. The definitions of the tunneling parameters J and F and of the on-site interaction energy parameter U are given in the Appendix. The coefficient $f_{3D} = 1-\alpha$ is obtained from the slope of the on-site interaction energy as a function of $\Delta N_k - N/N_c$. As shown in Refs. [18,20], the introduction of f_{3D} is crucial for obtaining an accurate dynamics. From this system of equations only $2N_c - 2$ are independent since the variables must fulfill $\sum_k n_k = 1$ and $\sum_k \varphi_k = 0$.

B. Localized states

In previous works, we have described in detail the method for obtaining the localized states in terms of GP stationary states [18,20,25]. Summarizing, first the stationary states $\psi_n(r,\theta,z)$ are obtained as the numerical solutions of the three-dimensional GP equation [26] with different winding numbers n, with n restricted to the values $-[(N_c-1)/2] \leqslant n \leqslant [N_c/2]$ [27] for large barrier heights [25]. Since the ψ_n are orthogonal for different n [20,25], one can define orthogonal WL functions localized on the k site by the following expression:

$$w_k(r,\theta,z) = \frac{1}{\sqrt{N_c}}\sum_n \psi_n(r,\theta,z)\,e^{-in\theta_k}, \tag{4}$$

with $\theta_k = 2\pi k/N_c$ for $-[(N_c-1)/2] \leqslant k \leqslant [N_c/2]$. A discussion of how to choose the global phases of $\psi_n(r,\theta,z)$ in order to achieve the maximum localization of w_k is given in Ref. [18].

In its turn, the stationary wave functions can be written in terms of the localized WL wave functions in Eq. (4) as

$$\psi_n(r,\theta,z) = \frac{1}{\sqrt{N_c}}\sum_k w_k(r,\theta,z)e^{in\,k\,2\pi/N_c}. \tag{5}$$

For the four-well problem, $N_c = 4$, the states with $n = \pm 1$ are degenerate and can be regarded as vortex-antivortex states since $\psi_{\pm 1} = \frac{1}{2}\sum_k w_k e^{\pm i\frac{\pi}{2}k}$ have opposite circulation. It is worth remarking that, as the GP equation is nonlinear, linear combinations of degenerate stationary states, e.g., the vortex-antivortex states, are in general nonstationary.

III. THE SYSTEM, TRAPPING POTENTIAL, AND PARAMETERS

Although the states investigated in this work also exist for larger numbers of wells, in our numerical simulations we consider a four-well ring-shaped trapping potential given by

$$\begin{aligned}V_{\rm trap}(\mathbf{r}) &= \frac{m}{2}\left[\omega_r^2 r^2 + \omega_z^2 z^2\right]\\ &\quad + V_b[\cos^2(\pi x/q_0) + \cos^2(\pi y/q_0)],\end{aligned} \tag{6}$$

where $r^2 = x^2 + y^2$ and m is the atomic mass. The harmonic frequencies are given by $\omega_r = 2\pi \times 70$ Hz and $\omega_z = 2\pi \times 90$ Hz, and the lattice parameter is $q_0 = 5.1\ \mu$m. Hereafter, time and energy are given in units of ω_r^{-1} and $\hbar\omega_r$, respectively. The length is given in units of the radial oscillator length $l_r = \sqrt{\hbar/(m\omega_r)} \simeq 1.3\ \mu$m. We also fix the barrier height parameter at $V_b = 25\hbar\omega_r$ and the number of particles to $N = 1\times10^4$.

For a system of rubidium atoms in the above configuration we have obtained the following multimode parameters: the hopping, $J = -6.60\times10^{-4}\hbar\omega_r$; the interaction-driven hopping parameter, $F = 2.08\times10^{-3}\hbar\omega_r$; the on-site interaction energy, $U = 3.16\times10^{-3}\hbar\omega_r$; and the effective on-site interaction energy $U_{\rm eff} = 2.27\times10^{-3}\hbar\omega_r$, being $\alpha = 0.28$. We numerically solve the GP equation on a grid of up to $512\times512\times256$ points and using a second-order split-step Fourier method for the dynamics with a time step of $\Delta t = 10^{-4}\omega_r^{-1}$. For more details see Ref. [18].

IV. THE STATES

In this section we first analyze a set of stationary points of the M model with equally populated sites whose associated order parameters are in general not exact GP stationary states. These states will be called peculiar. In a second step, we show that for states with conveniently chosen initial occupation numbers and the same distribution of initial phases as the peculiar states, the populations remain blocked during all the evolution. The properties of such BON states are studied next.

A. Peculiar stationary states

The GP stationary states used for constructing the multimode model give rise to stationary points in the M model. However, in addition to these standard points, we found a peculiar set of stationary points in a condensate with $N_c = 4l$ sites. These states are defined by $|b_k| = 1/\sqrt{N_c}$ and the following local phases: $\phi_0 = 0$, $\phi_1 = f_0 - \pi$, $\phi_2 = \pi$, and $\phi_{-1} = f_0$ for a four-well trap ($l = 1$). However, for larger l, the sequence of phases is repeated l times along the ring. We refer to these states as peculiar because f_0 could take any value, so instead of having isolated points in the phase diagram we have a continuous family of stationary points parametrized by f_0. This family contains the two stationary points $f_0 = \pm\pi/2$ which correspond to singly quantized vortex states, namely, GP stationary states with winding numbers ±1. In Fig. 1(a) a scheme of the trap and the condensate is depicted qualitatively showing states with different populations, and in Fig. 1(b) the localized WL function in the $z = 0$ plane is shown together with the peculiar initial phases.

We further investigate if the peculiar order parameter could also be another stationary solution of the GP equation [26],

$$\left[-\frac{\hbar^2}{2m}\nabla^2 + V_{\rm trap} + gN|\psi(\mathbf{r})|^2\right]\psi(\mathbf{r}) = \mu\,\psi(\mathbf{r}), \quad (7)$$

where μ is the chemical potential and $g = 4\pi\hbar^2 a/m$ is the interaction strength among atoms with a being their s-wave scattering length.

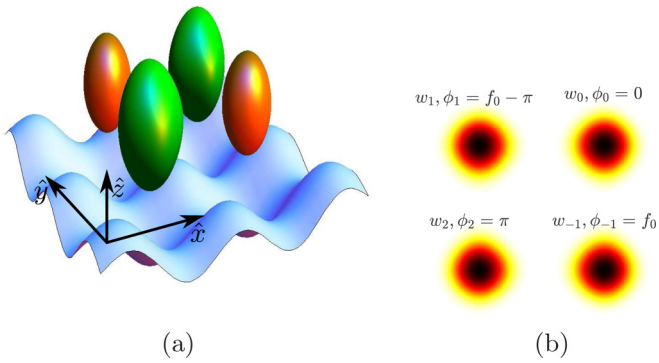

FIG. 1. (a) Schematic three-dimensional states density and the trapping potential of the four-site system (in arbitrary units). (b) Localized states w_k at the plane $z = 0$; also the peculiar set of initial values of the phases are indicated.

The normalized-to-unity order parameter associated to the peculiar points reads

$$\psi_M(\mathbf{r}, t) = \tfrac{1}{2}[w_0(\mathbf{r}) - w_2(\mathbf{r})] - \tfrac{1}{2}[w_1(\mathbf{r}) - w_{-1}(\mathbf{r})]e^{if_0}, \quad (8)$$

which in terms of GP stationary states can be written as

$$\psi_M(\mathbf{r}) = \tfrac{1}{2}[(1 + ie^{if_0})\psi_1(\mathbf{r}) + (1 - ie^{if_0})\psi_{-1}(\mathbf{r})]. \quad (9)$$

The peculiar states are therefore a superposition of vortex states with opposite circulation. Since the states $\psi_1(\mathbf{r})$ and $\psi_{-1}(\mathbf{r})$ have the same chemical potential $\mu_1 = \mu_{-1}$ and verify $\psi_1(\mathbf{r}) = \psi^*_{-1}(\mathbf{r})$, applying the GP equation (7) to ψ_M, we obtain

$$\left[-\frac{\hbar^2}{2m}\nabla^2 + V_{\rm trap} + gN|\psi_M(\mathbf{r})|^2\right]\psi_M(\mathbf{r}) = \mu_1\,\psi_M(\mathbf{r}) - gN\cos(f_0)\mathrm{Im}\big(\psi_1^2(\mathbf{r})\big) \times [\mathrm{Re}(\psi_1) - \mathrm{Im}(\psi_1)e^{if_0}], \quad (10)$$

where, in addition, we have that

$$\mathrm{Im}\big(\psi_1^2(\mathbf{r})\big) = \tfrac{1}{4}[w_0(\mathbf{r}) - w_2(\mathbf{r})]\,[w_1(\mathbf{r}) - w_{-1}(\mathbf{r})] \quad (11)$$

is almost vanishing if the WL functions are well localized as in the present case. Therefore, these peculiar stationary points can be regarded as quasistationary solutions of the GP equation.

For the particular case of $f_0 = \pm\pi/2$, the second term on the right-hand side of Eq. (10) vanishes and thus the order parameter is an exact solution of the GP equation. Otherwise, a general value of f_0 generates an entire continuous family of states that shows a collective motion independent of time. The $\psi_{\pm1}$ stationary solutions can be regarded as particular cases of Eq. (9) with maximum angular momentum. On the other hand, for $f_0 = 0$ we have $\psi_M(\mathbf{r}) = \frac{1}{2}[(1 + i)\psi_1(\mathbf{r}) + (1 - i)\psi_{-1}(\mathbf{r})]$ which is real; hence, its angular momentum is zero. Nevertheless, an active vortex dynamics is present, due to the nonzero circulation of $\psi_{\pm1}$. The same holds for $f_0 = \pi$.

We want to remark that such a family of stationary solutions of the M model does not necessarily exist in ring lattices with an arbitrary number of wells as it can be straightforwardly deduced from the dynamical equations (2) and (3). For example, for $N_c = 3$ even though the degenerate stationary

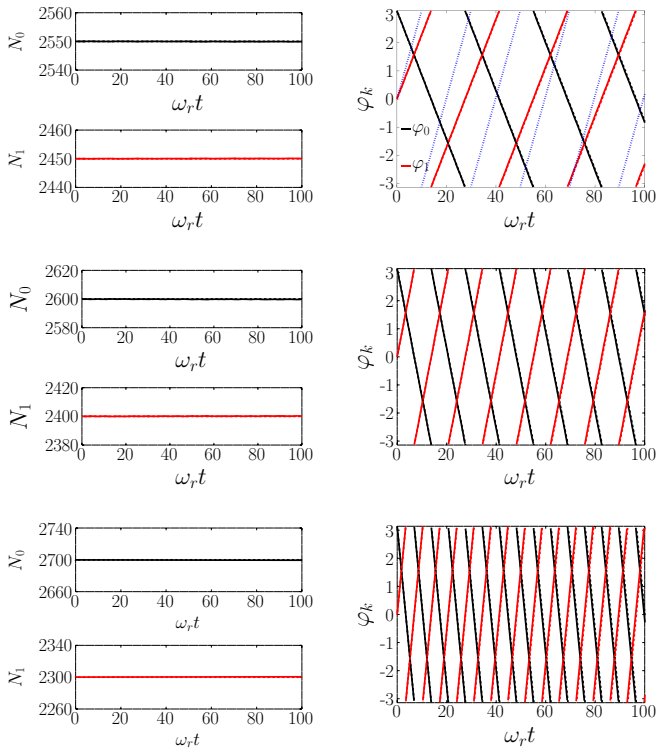

FIG. 2. Populations (left column) and phase differences (right column) as function of time, from top to bottom for $\Delta N = 100$, 200, and 400 with $f_0(0) = -\pi$. The solid lines correspond to GP simulations and the dashed lines to the M model. Black and red lines correspond to N_k and φ_k with $k = 0$ and $k = 1$, respectively. The dotted blue lines in the top right illustrate the prediction of the M model with the bare U for $k = 1$.

states with winding numbers $n = \pm 1$ are also present, the corresponding stationary points in the phase diagram only exist as isolated points.

B. Nonstationary BON states

When the numbers of particles of alternate sites are equal and the phases maintain their peculiar relation, $\phi_0 = 0$, $\phi_1 = f_0 - \pi$, $\phi_2 = \pi$, and $\phi_{-1} = f_0$, the site populations do not evolve. This condition gives rise to very special dynamical states where f_0 becomes time dependent. This is shown in Fig. 2, where we compare the evolution of the occupation numbers and phase differences using full three-dimensional GP simulations with the dynamics arising from the M model. The selected initial population differences, from top to bottom, are $\Delta N = 100$, 200, and 400, where $\Delta N = N_0 - N_1$ and $f_0(0) = -\pi$. From Fig. 2 it may be seen that in all cases the number of particles in each site remains fixed in time, whereas their phase differences evolve faster for larger imbalances. We have further investigated the GP equation (GPE) dynamics for imbalances up to $\Delta N = 3\times10^3$ and verified that the populations remain constant within 0.1% accuracy.

This family of states bears some resemblance to self-trapped states; however, there are many important differences compared to the well-known ST dynamics in double-well potentials. First of all, the population imbalance can be arbitrarily small. Instead, to reach these states, it is only necessary to achieve the peculiar phases described above, $f_0(0)$ being an arbitrary value (given that $n_k = n_{k+2}$). Second, the hopping parameters J and F play no role in the dynamics; hence, we cannot associate the emergence of the BON states to the small enough tunneling energy splitting like in the ST regime in two wells [9].

The BON state normalized to unity reads

$$\psi_M(\mathbf{r},t) = \sqrt{n_0}[w_0(\mathbf{r}) - w_2(\mathbf{r})] - \sqrt{n_1}[w_1(\mathbf{r}) - w_{-1}(\mathbf{r})]e^{if_0(t)}, \quad (12)$$

which, written in terms of GP stationary states, yields

$$\psi_M(\mathbf{r}) = (\sqrt{n_0} + i\sqrt{n_1}e^{if_0(t)})\psi_1(\mathbf{r}) + (\sqrt{n_0} - i\sqrt{n_1}e^{if_0(t)})\psi_{-1}(\mathbf{r}). \quad (13)$$

In order to obtain $f_0(t)$ one can rewrite Eqs. (3) and extract the evolution of $f_0(t)$ from $\hbar\dot{\varphi}_k = (n_{k-1} - n_k)NU_{\rm eff}$. This yields

$$f_0(t) = \frac{1}{\hbar}U_{\rm eff}\Delta N\, t + f_0(0), \quad (14)$$

which in turns completely defines all the phase differences at any time within the M model. In particular, we have $\varphi_0(t) = -f_0(t)$ and $\varphi_1(t) = f_0(t) - \pi$. We note that for $n_0 = n_1$ the state (13) coincides with the peculiar state (9).

It is important to point out here that the perfect agreement between the results of the GP equation and the M model observed in Fig. 2 is due to the proper definition of the on-site interaction energy parameter $U_{\rm eff} = 2.27\times10^{-3}\hbar\omega_r$ [19,20], instead of using the bare value $U = 3.16\times10^{-3}\hbar\omega_r$. To illustrate such a difference, we included in Fig. 2 the evolution of $\varphi_1(t)$ for $\Delta N = 100$ using the bare parameter U. Hence, we confirm the accuracy on the calculation of the effective on-site interaction energy parameter also in this dynamical regime.

To conclude we note that using Eq. (14) one can obtain the time period for the phase differences,

$$T_M = \frac{2\pi\hbar}{U_{\rm eff}\Delta N}, \quad (15)$$

which turns out to be also the time period of the persistent and collective oscillation around the ring.

1. Angular momentum

An additional evidence of this dynamical regime is reflected in the time evolution of other observables. In particular, we show that within the M model the angular momentum exhibits a sinusoidal behavior as a function of time with a period T_M.

The expectation value per particle of a general observable $\widehat{O}$, considering an arbitrary state in the M model, is given by

$$\langle\widehat{O}\rangle = \sum_k n_k\langle w_k|\widehat{O}|w_k\rangle + 2\sum_k\sqrt{n_k n_{k+1}}\,{\rm Re}[e^{i(\phi_k-\phi_{k+1})}\langle w_{k+1}|\widehat{O}|w_k\rangle]. \quad (16)$$

Since each well is equivalent to all others, except for a discrete rotation, we have $\langle w_k|\widehat{O}|w_k\rangle = \langle w_0|\widehat{O}|w_0\rangle$ and

$\langle w_{k+1}|\widehat{O}|w_k\rangle = \langle w_1|\widehat{O}|w_0\rangle$ for all k. Hence, the expectation value becomes

$$\langle\widehat{O}\rangle = \langle w_0|\widehat{O}|w_0\rangle + 2\sum_k \sqrt{n_k n_{k+1}}\,\mathrm{Re}[e^{-i\varphi_{k+1}}\langle w_1|\widehat{O}|w_0\rangle]. \quad (17)$$

For the z component of the angular momentum we have $\widehat{O} = \widehat{L}_z = -i\hbar\frac{\partial}{\partial\theta}$ and then, taking into account that the localized states can be chosen as real functions, one obtains the expectation value of angular momentum:

$$\langle\widehat{L}_z\rangle = -2\hbar\langle w_1|\frac{\partial}{\partial\theta}|w_0\rangle\sum_k\sqrt{n_k n_{k+1}}\sin\varphi_{k+1}. \quad (18)$$

In a BON state with initial condition $f_0(0) = -\pi$, as $\sin\varphi_k = -\sin f_0(t)$ for every k, we can write

$$\langle\widehat{L}_z\rangle = -8\hbar\sqrt{n_0 n_1}\langle w_1|\frac{\partial}{\partial\theta}|w_0\rangle\sin\left(\frac{1}{\hbar}U_{\mathrm{eff}}\Delta N t\right), \quad (19)$$

where the bracket involving the localized states is a negative number. As expected, the period of this sinusoidal function is T_M. Furthermore, one can see that the stationary state Eq. (8), corresponding to $\Delta N = 0$, yields a constant angular momentum proportional to $\sin(f_0)$.

2. *Underlying dynamics*

Although the population in each well remains completely fixed, the order parameter evolves in time and exhibits spatial oscillations. In order to analyze such a dynamics we first investigate the evolution of the density profile. Using the BON state expression given by Eq. (12), the evolution of the density $\rho_M(\mathbf{r},t) = |\psi_M(\mathbf{r},t)|^2$ within the M model is given by

$$\frac{\partial\rho_M(\mathbf{r},t)}{\partial t} = 2\sqrt{n_0 n_1}\,\dot{f}_0(t)\,\sin f_0(t) \times[w_0(\mathbf{r}) - w_2(\mathbf{r})][w_1(\mathbf{r}) - w_{-1}(\mathbf{r})], \quad (20)$$

with $\hbar\dot{f}_0(t) = U_{\mathrm{eff}}\Delta N$ [cf. Eq. (14)]. Equation (20) implies that $\rho_M(\mathbf{r},t)$ is approximately stationary within each well, where the overlap between the WL functions of neighboring sites is negligible, whereas the density variations are confined to the interwell regions or junctions where the localized states do overlap. Moreover, one can infer the change of sign of $\partial\rho_M(\mathbf{r},t)/\partial t$ at the junctions by analyzing Eq. (20). One can thus conclude that particles oscillate across both junctions of a given site without changing its net population. Furthermore, the maximum and minimum density variations during the evolution occur at times t_M and t_m when $f_0(t_M) = 0$ and $f_0(t_m) = \pi$, respectively.

The sense of the particles' flow across the junctions can be read off from the spatial profiles of the phases $\phi(\mathbf{r},t)$ of the wave function. In Fig. 3 we show snapshots of these phases at several times in the $z = 0$ plane obtained from both $\psi_M(\mathbf{r},t)$ and $\psi_{\mathrm{GP}}(\mathbf{r},t)$ in the left and right panels, respectively. In both cases we have subtracted a global phase $\phi_0(t)$ from $\phi(\mathbf{r},t)$ in order to better observe the dynamics. The initial condition is $\Delta N = 200$ and $f_0 = -\pi$, which yield a multimode period $T_M \simeq 13.8\omega_r^{-1}$, in sharp contrast to $2\pi\hbar/(U\Delta N) = 9.95\omega_r^{-1}$ that would be obtained with the bare on-site interaction.

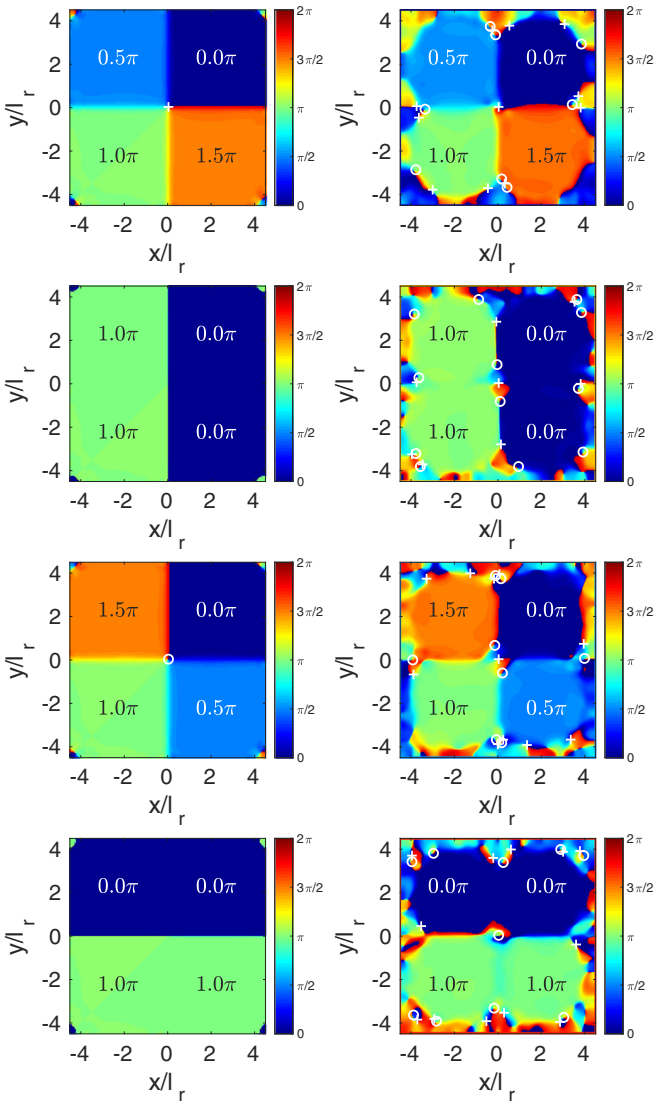

FIG. 3. Phase snapshots at the $z = 0$ plane obtained from the M model (left column) and from GP simulations (right column) for $\Delta N = 200$. The coordinates x and y are divided by $l_r = \sqrt{\hbar/(m\omega_r)}$. The GP times, from top to bottom on the right column, correspond to $t_a = 3.4\omega_r^{-1}$, $t_b = 6.9\omega_r^{-1}$, $t_c = 10.3\omega_r^{-1}$, and $t_d = 13.7\omega_r^{-1}$. The plus signs (open circles) indicate the vortex (antivortex) locations. The indicated phase values correspond to the local phases evaluated at each site center.

In the left-hand column, from top to bottom, we show the phase $\phi_M(\mathbf{r},t)$ obtained from the order parameter $\psi_M(\mathbf{r},t)$ for the aforementioned configurations at several times: (a) at $t = T_M/4$ ($f_0 = -\pi/2$), there is a $\pi/2$ difference between neighboring sites and the velocity field corresponds to that of a vortex with a phase gradient in the counterclockwise direction; (b) at $t = T_M/2$ ($f_0 = 0$), the phase difference between the right and left sites is π, which corresponds to a vanishing velocity field; (c) at $t = 3T_M/4$ ($f_0 = \pi/2$), there is a $-\pi/2$ difference between neighboring sites, the circulation being clockwise as for an antivortex; and finally, (d) at $t = T_M$ ($f_0 = \pi$), there is a π phase difference between the top and bottom sites. In the figure we have marked with a plus symbol

and with an open circle the presence of a vortex and an antivortex, respectively. For the M model, it can be seen that, in the left column of Fig. 3, there exists a vortex and an antivortex at the origin for the configurations (a) $t = T_M/4$ and (c) $t = 3/4T_M$, in agreement with the distributions described above. In the model, the vortex (antivortex) remains fixed at $x = 0$, $y = 0$ during the interval $0 < t < T_M/2$ ($T_M/2 < t < T_M$).

On the other hand, in the right-hand column of Fig. 3 we show phase snapshots obtained from full three-dimensional (3D) GP simulations for times near the four different situations previously discussed. We have observed that the GP evolutions incorporate additional fluctuations and hence the velocity circulation does not change exactly at quarters of the period T_M. Moreover, the velocity field never vanishes, as the change of its circulation is associated with a passage of vortices instead of with the appearance of a nodal surface [6]. Nevertheless, as shown together in Fig. 3, the order parameter from the M model is able to capture rather accurately the spatial distribution of phases present in the exact GP dynamics.

In particular, from top to bottom in Fig. 3, we show the results for the GP times: $t_a = 3.4\omega_r^{-1}$, $t_b = 6.9\omega_r^{-1}$, $t_c = 10.3\omega_r^{-1}$, and $t_d = 13.7\omega_r^{-1}$. In each site we indicate the value of the local phase $\phi_{\rm GP}(\mathbf{r}, t)$ evaluated at the center of the corresponding well to be compared with that obtained in the M model. It may be confirmed that at every time the phase difference between alternated sites is always π as predicted by the model.

It becomes clear from the change of sign in the phase differences that the velocity field is inverted near each half period, when the extreme variations in the density at the junctions are achieved. Except for some fluctuations around such a transition, in the intermediate times the total topological charge is conserved, whereas the number and the position of the vortices may change. In particular, in the third row of the right-hand column of Fig. 3, one vortex and two antivortices are observed with a total negative charge of -1 instead of the single fixed antivortex predicted by the M model.

It is worthwhile to recall that the velocity circulation is quantized along any closed curve inside the superfluid and, as established in the celebrated Helmholtz-Kelvin theorem [28], it is conserved during the evolution if the superfluid condition is not broken [29]. As a consequence, the value of the circulation can only change when a vortex passes through the curve (phase slip) or when the density goes to zero.

Although both the GP equation and the M model must obey the Helmholtz-Kelvin theorem, the order parameter given by the multimode model cannot predict the motion of vortices or the generation of vortex-antivortex pairs; hence, the change of the velocity field circulation could be only provided through the appearance of nodal surfaces. The nodal surfaces arise when the minimum in the local density is achieved, i.e., at $f_0 = 0, \pi$. For example, at $f_0 = 0$ the order parameter in Eq. (12) reduces to

$$\psi_M(\mathbf{r}) = \sqrt{n_0}[w_0(\mathbf{r}) - w_2(\mathbf{r})] - \sqrt{n_1}[w_1(\mathbf{r}) - w_{-1}(\mathbf{r})], \tag{21}$$

which corresponds to the second configuration on the left-hand column of Fig. 3. If all the populations were equal this condition would lead to the $x = 0$ plane. In our case, the deviation from a plane is due to the difference in the populations. The intersection of the nodal surface with the plane $z = 0$ can be viewed in the graph by the sharp π change of the phase where the density goes to zero. Similarly, one can obtain the nodal surfaces for $f_0 = \pi$, which corresponds to the fourth configuration. In this case the curve where the density goes to zero is around $y = 0$.

In contrast with the M model, the change of the velocity circulation in the GP frame is produced by the dynamics of vortices passing through the potential barriers and may include generation of vortex-antivortex pairs. In fact, we have observed that several vortex-antivortex pairs may be spontaneously generated along the barriers, thus simulating a density closer to that of the M model nodal surface. This active dynamics of vortices around the transitions is produced in a timescale much smaller than T_M and hence it is not possible to access the details of the vortex motion within the present numerical precision. As an illustration, we note that the last time of the depicted GP snapshots is slightly smaller than the T_M period and there still exists an antivortex around the center of the system.

3. Velocity field circulation

Taking into account the previous findings for the multimode model one can conclude that in one T_M period the system passes through a sequence of phases that yields an alternating velocity field circulation between values 1 and -1 along a curve that connects the four wells. The transition between these two values occurs at $f_0 = 0$ and $f_0 = \pi$ when the order parameter develops a nodal surface. In Fig. 4 we show the velocity field circulation $\mathcal{C} = \oint \mathbf{v} \cdot d\mathbf{r}$ as a function of time using the M model and GP simulations. It may be seen that the same behavior is observed with both approaches. The M model is thus able to reproduce the behavior of the circulation although the details of the internal vortex dynamics is lost. In the GP dynamics the change of circulation is caused by the motion of vortices together with the creation or annihilation of vortex-antivortex pairs. Signatures of such a vortex dynamics could be observed in Fig. 3 where we have shown the phases around the transition. Another evidence of a vortex dynamics can also be visualized in the middle panel of Fig. 4, where an additional change of sign is produced near the transition.

4. Stability analysis

In this section we investigate the stability of the BON states by means of a Floquet analysis [18,30] of the multimode dynamical equations. This analysis is based on the characterization of the linear dynamics around its periodic orbits. In our case, the BON states are periodic solutions with constant populations $n_i(t) = n_i$ and linear phase differences $\varphi_i(t) = \varphi_i^0 + (-1)^{i+1} 2\pi\, t/T_M$, where φ_i^0 fulfill the relations $\varphi_0^0 = -f_0(0)$, $\varphi_1^0 = f_0(0) - \pi$, $\varphi_2^0 = 2\pi - f_0(0)$, and $\varphi_{-1}^0 = f_0(0) - \pi$. The linearization of the dynamics around these states yields the nonautonomous system

$$\frac{d\boldsymbol{\delta}}{dt} = \mathbb{A}[n_i(t), \varphi_i(t)]\Big|_{\rm BON} \cdot \boldsymbol{\delta}(t), \tag{22}$$

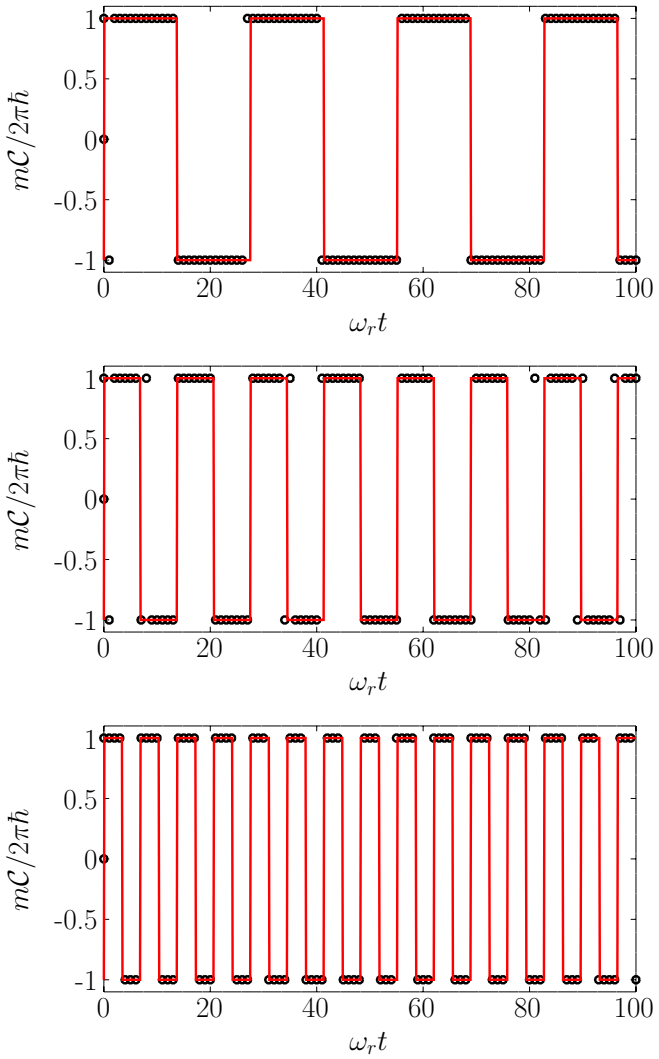

FIG. 4. Velocity field circulation $\mathcal{C}$ (in units of $2\pi\hbar/m$) as a function of time for $\Delta N = 100$, 200, and 400 (from top to bottom). The circles correspond to the GP results while the solid line corresponds to the results from the M model. The circulation was calculated along a square that connects the centers of the four sites in the $z = 0$ plane.

where $\boldsymbol{\delta}$ is a vector comprising both density and phase-difference fluctuations. As the BON states correspond to symmetric initial populations with peculiar phases, it is natural to consider as variables $\boldsymbol{\delta}$ the departures from a symmetric case; namely, we define

$$\delta_1 = (n_0 - n_2)/2, \quad \delta_2 = (n_1 - n_{-1})/2, \tag{23}$$

$$\delta_3 = (\varphi_0 - \varphi_2)/2 + \pi, \quad \delta_4 = (\varphi_1 - \varphi_{-1})/2. \tag{24}$$

Given that the matrix $\mathbb{A}$ has a period T_M, the linearized dynamics can be characterized by the so-called Monodromy matrix $\mathbb{M}$ which contains the change of $\boldsymbol{\delta}$ after one period, i.e., $\mathbb{M} \cdot \boldsymbol{\delta}(0) = \boldsymbol{\delta}(T_M)$. The matrix is built from the solutions of Eq. (22) with canonical initial conditions evaluated at T_M [18,30]. In Fig. 5 we depict elements of $\mathbb{M}$ showing the effect of an initial population fluctuation. The orbits are regular if the perturbed system remains near the initial one after a period.

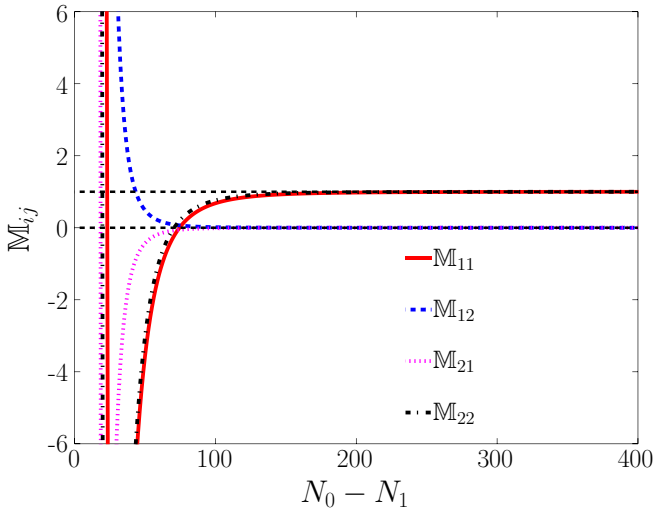

FIG. 5. Selected elements of the Monodromy matrix $\mathbb{M}_{ij}$ as functions of the particle imbalance $N_1 - N_2$ of BON states with $f_0(0) = \pi$. The horizontal dashed lines mark the values $\mathbb{M}_{ij} = 0, 1$.

This happens when $\mathbb{M}_{ii} \simeq 1$ and $\mathbb{M}_{i\neq j} \simeq 0$. On the contrary, when the fluctuations are enhanced ($|\mathbb{M}_{ij}| \gg 1$), the orbits are unstable. This may be observed in Fig. 5 for low imbalances.

For the peculiar stationary states ($\Delta N = 0$), the linear system is time independent and the problem reduces to a straightforward diagonalization of $\mathbb{A}$ to obtain the excitation frequencies $\tilde{\omega}$ corresponding to the Bogoliubov collective modes in the case of the full GPE. The four frequencies are found to be

$$\tilde{\omega} = \pm\sqrt{F^2 \cos^2 f_0 \pm K\frac{NU_{\text{eff}}}{2}\cos f_0 - (K+F)^2}, \tag{25}$$

where $K = 2J + F$. As $NU_{\text{eff}} \gg K, F$, the most stable frequency for a given system is attained for peculiar states with $f_0 = \pm\pi/2$, which in turn yield an imaginary frequency $\tilde{\omega}^2 = -(K+F)^2$. Therefore, all f_0 give rise to dynamically unstable peculiar states. The stability of stationary vortex states ($f_0 = \pm\pi/2$) has been previously investigated in [31] for circular arrays of Bose-Einstein condensates, finding that only states with circulation below $N_c/4$ are stable.

5. Proposed experimental test

The correct preparation of BON states requires a special sequence of phases and symmetric initial populations ($n_k = n_{k+1}$). While the common approach to experimentally measure both of them is by means of time-of-flight (TOF) and absorption images, the simple dynamics of BON states offers an alternative way to confirm its correct realization using TOF images only. Given that the relative phases among neighboring sites are revealed in the interference patterns during the TOF expansion [9], it could be verified that they obey the peculiar sequence of phases at all times. According to Eq. (14), in this case $f_0(t)$ must be a linear function whose slope γ relates to the particle imbalance as

$$\Delta N = \frac{\hbar\gamma}{U_{\text{eff}}}, \tag{26}$$

which might prove to be a more accurate measure than the direct estimate from absorption images. On the other hand, since Eq. (26) requires the use of $U_{\rm eff}$ instead of the bare U, it may also serve to confirm its numerical value. By using U the relative error on the imbalances could be as large as of order 20–30 %, depending on the number of particles [7].

Due to the experimental uncertainty, absorption images may not be able to reveal a slightly broken symmetry of the population configuration. However, the evolution of the phases will depart from linearity and will not be determined by the single function f_0.

V. EXTENSION TO LARGER NUMBER OF WELLS

It is possible to extend the peculiar and BON states to a larger number of wells provided the sequence of phases $\ldots, 0, f_0-\pi, \pi, f_0, 0, \ldots$ is repeated $l = N_c/4$ times around the ring lattice, and the populations alternate between two values, with $n_{2k} = n_0$ and $n_{2k+1} = n_1$. This is only possible when the numbers of wells are multiples of 4. Taking into account these conditions in Eq. (1) and using Eq. (4) to eliminate the WL functions w_k, we can write the following BON order parameter in terms of GP stationary states:

$$\psi_M(\mathbf{r}) = \frac{\sqrt{N_c}}{2}\big[(\sqrt{n_0} + i\sqrt{n_1}e^{if_0(t)})\psi_{\frac{N_c}{4}}(\mathbf{r}) + (\sqrt{n_0} - i\sqrt{n_1}e^{if_0(t)})\psi_{-\frac{N_c}{4}}(\mathbf{r})\big]. \quad (27)$$

It is straightforward to show that $f_0(t)$ still obeys Eq. (14), and thus the corresponding time period is also given by Eq. (15). Therefore, the analysis performed in the previous section can be repeated using the same procedure, including the Floquet theory. However, for these configurations the velocity field circulation alternates between $\pm N_c/4$ and the number of nodal surfaces at each half period is equal to l. Equation (27) shows that an arbitrary linear combination of $\psi_{\pm\frac{N_c}{4}}$ leads to the BON dynamics. For example, even though for $N_c = 8$ it is not possible to generate the BON dynamics with a linear combination of the degenerate $\psi_{\pm1}$ states; any linear combination of $\psi_{\pm2}$ will indeed give rise to a BON dynamics.

Using Eq. (18) the mean value of the z component of the angular momentum is given by

$$\langle L_z\rangle(t) = 2N_c\hbar\langle w_1|\frac{\partial}{\partial\theta}|w_0\rangle\sqrt{n_0 n_1}\sin(f_0(t)). \quad (28)$$

If we let $n_0 = n_1$ then we obtain the most general quasistationary states described in Sec. IV A:

$$\psi_M(\mathbf{r}) = \tfrac{1}{2}\big[(1+ie^{if_0})\psi_{\frac{N_c}{4}}(\mathbf{r}) + (1-ie^{if_0})\psi_{-\frac{N_c}{4}}(\mathbf{r})\big], \quad (29)$$

which satisfies

$$\Big[-\frac{\hbar^2}{2m}\nabla^2 + V_{\rm trap} + gN|\psi_M(\mathbf{r})|^2\Big]\psi_M(\mathbf{r}) = \mu_{\frac{N_c}{4}}\,\psi_M(\mathbf{r}) - gN\cos(f_0)\mathrm{Im}\big(\psi^2_{\frac{N_c}{4}}(\mathbf{r})\big) \times\big[\mathrm{Re}\big(\psi_{\frac{N_c}{4}}\big) - \mathrm{Im}\big(\psi_{\frac{N_c}{4}}\big)e^{if_0}\big]. \quad (30)$$

Since

$$\mathrm{Im}\big(\psi^2_{\frac{N_c}{4}}\big) = \frac{1}{N_c}\sum_{k,k'} w_k w_{k'}\sin\Big[\frac{\pi}{2}(k+k')\Big], \quad (31)$$

the states in Eq. (29) can be regarded as quasistationary solutions of the GP equation when the w_k are well-localized functions.

VI. SUMMARY AND CONCLUDING REMARKS

We have studied a particular dynamical regime of a Bose-Einstein condensate in a ring-shaped lattice which possesses a set of states with fixed number of particles in each site and a simple dynamics in their phases. The same distribution of phases along the sites that gives rise to such nonstationary states has been shown to generate a continuous family of stationary points in the phase space of the multimode model. Such peculiar states have constant nonzero angular momentum, when all the populations are equal, and include two states that correspond to exact GP stationary solutions.

We have shown that the nonlinearity of the GP equation governs the dynamics within this regime and that it is responsible for the population blocking in the nonstationary states. In contrast to the self-trapping phenomenon this effect does not possess a lower bound for the population imbalance.

We have studied the time evolution of BON states using both the multimode model and the three-dimensional GP equation, finding an excellent agreement in the populations in each site and in their phase differences. This accuracy was possible due to the inclusion of the effective interaction energy parameter instead of the bare one. Even though the multimode model was unable to account for the motion of individual vortices and the creation or annihilation of vortex-antivortex pairs, it was demonstrated that it correctly predicts the evolution of the velocity circulation and angular momentum, characterizing this regime as a persistent current oscillating around the lattice.

By performing a Floquet stability analysis of the blocked population states, we have verified that their dynamics is regular for the particle imbalances here considered. In a four-well system these states could, in principle, be experimentally achieved by initially manipulating the position of the potential barriers in order to have different populations or by using an elliptic trap in the (x, y) plane with their axis forming a $\pi/4$ angle during a short time and then reverting the potential to a circular harmonic trap. A simple way to produce the initial distribution of phases would be to start with the same state as we have used in our numerical calculations. This could be achieved by illuminating half of the condensate (e.g., $x > 0$) with an additional laser for a period of time until it develops a π phase difference between the half spaces $x > 0$ and $x < 0$. However, any other initial distribution of phases seems feasible using a spatial light modulator (SLM) [32–34], and hence also the whole family of stationary M-model states could be directly generated. Furthermore, given that all the phases lose their dependence on a single linear function as soon as the symmetric condition on the site populations is lifted, these states could be first tested to adjust the population in alternate wells with arbitrary imbalances. A second phase imprinting application could then be used to generate the desired state.

Since the BON states present a simple analytical form for the phase difference between neighboring sites, it could also allow one to measure the initial population imbalance by means of interference patterns in TOF images, rather than absorption images.

ACKNOWLEDGMENTS

This work was supported by CONICET and Universidad de Buenos Aires through Grants No. PIP 11220150100442CO and No. UBACyT 20020150100157BA, respectively.

APPENDIX: PARAMETERS

The multimode model parameters are defined by

$$J = -\int d^3\mathbf{r}\; w_0(\mathbf{r})\left[-\frac{\hbar^2}{2m}\nabla^2 + V_{\text{trap}}(\mathbf{r})\right] w_1(\mathbf{r}), \tag{A1}$$

$$U = g\int d^3\mathbf{r}\; w_0^4(\mathbf{r}), \quad \text{and} \tag{A2}$$

$$F = -N\,g\int d^3\mathbf{r}\; w_0^3(\mathbf{r}) w_1(\mathbf{r}). \tag{A3}$$

Together with the calculation of these parameters by the preceding definitions we have followed the alternative method outlined in Ref. [20] which involves directly the energies of the GP stationary states. Both approaches have proven to yield values equal in less than 1%. We note that we have disregarded the parameter that involves products of neighboring densities because, for the present system, its contribution turned out to be negligible.

[1] A. Smerzi, S. Fantoni, S. Giovanazzi, and S. R. Shenoy, Phys. Rev. Lett. **79**, 4950 (1997).

[2] S. Raghavan, A. Smerzi, S. Fantoni, and S. R. Shenoy, Phys. Rev. A **59**, 620 (1999).

[3] D. Ananikian and T. Bergeman, Phys. Rev. A **73**, 013604 (2006).

[4] X. Y. Jia, W. D. Li, and J. Q. Liang, Phys. Rev. A **78**, 023613 (2008).

[5] M. Melé-Messeguer, B. Juliá-Díaz, M. Guilleumas, A. Polls, and A. Sanpera, New J. Phys. **13**, 033012 (2011).

[6] M. Abad, M. Guilleumas, R. Mayol, M. Pi, and D. M. Jezek, Europhys. Lett. **94**, 10004 (2011).

[7] M. Nigro, P. Capuzzi, H. M. Cataldo, and D. M. Jezek, Eur. Phys. J. D **71**, 297 (2017).

[8] T. Mayteevarunyoo, B. A. Malomed, and G. Dong, Phys. Rev. A **78**, 053601 (2008); B. Xiong, J. Gong, H. Pu, W. Bao, and B. Li, *ibid.* **79**, 013626 (2009); Qi Zhou, J. V. Porto, and S. Das Sarma, *ibid.* **84**, 031607(R) (2011); B. Cui, L. C. Wang, and X. X. Yi, *ibid.* **82**, 062105 (2010); M. Abad, M. Guilleumas, R. Mayol, M. Pi, and D. M. Jezek, *ibid.* **84**, 035601 (2011).

[9] M. Albiez, R. Gati, J. Fölling, S. Hunsmann, M. Cristiani, and M. K. Oberthaler, Phys. Rev. Lett. **95**, 010402 (2005).

[10] Michael Albiez, Ph.D. thesis, University of Heidelberg, 2005.

[11] Rudolf Gati, Ph.D. thesis, University of Heidelberg, 2007.

[12] Th. Anker, M. Albiez, R. Gati, S. Hunsmann, B. Eiermann, A. Trombettoni, and M. K. Oberthaler, Phys. Rev. Lett. **94**, 020403 (2005).

[13] Bingbing Wang, Panming Fu, Jie Liu, and Biao Wu, Phys. Rev. A **74**, 063610 (2006).

[14] C. E. Creffield, Phys. Rev. A **75**, 031607(R) (2007); Ju-Kui Xue, Ai-Xia Zhang, and Jie Liu, *ibid.* **77**, 013602 (2008); T. J. Alexander, E. A. Ostrovskaya, and Y. S. Kivshar, Phys. Rev. Lett. **96**, 040401 (2006); Bin Liu, Li-Bin Fu, Shi-Ping Yang, and Jie Liu, Phys. Rev. A **75**, 033601 (2007).

[15] S. K. Adhikari, J. Phys. B: At. Mol. Opt. Phys. **44**, 075301 (2011).

[16] S. De Liberato and C. J. Foot, Phys. Rev. A **73**, 035602 (2006).

[17] G. Arwas, A. Vardi, and D. Cohen, Phys. Rev. A **89**, 013601 (2014).

[18] M. Nigro, P. Capuzzi, H. M. Cataldo, and D. M. Jezek, Phys. Rev. A **97**, 013626 (2018).

[19] D. M. Jezek, P. Capuzzi, and H. M. Cataldo, Phys. Rev. A **87**, 053625 (2013).

[20] D. M. Jezek and H. M. Cataldo, Phys. Rev. A **88**, 013636 (2013).

[21] R. Kolovsky, New J. Phys. **8**, 197 (2006).

[22] A. Gallemí, M. Guilleumas, J. Martorell, R. Mayol, A. Polls, and B. Juliá-Díaz, New J. Phys. **18**, 075005 (2016).

[23] A. Burchianti, C. Fort, and M. Modugno, Phys. Rev. A **95**, 023627 (2017).

[24] K. Henderson, C. Ryu, C. MacCormick, and M. G. Boshier, New J. Phys. **11**, 043030 (2009).

[25] H. M. Cataldo and D. M. Jezek, Phys. Rev. A **84**, 013602 (2011).

[26] E. P. Gross, Nuovo Cimento **20**, 454 (1961); L. P. Pitaevskii, Zh. Eksp. Teor. Fiz. **40**, 646 (1961) [Sov. Phys. JETP **13**, 451 (1961)].

[27] D. M. Jezek and H. M. Cataldo, Phys. Rev. A **83**, 013629 (2011).

[28] L. D. Landau and E. M. Lifshitz, *Fluid Mechanics* (Butterworth-Heinemann, New York, 1995).

[29] B. Damski and K. Sacha, J. Phys. A: Math. Gen. **36**, 2339 (2003).

[30] C. Chicone, *Ordinary Differential Equations with Applications*, 2nd ed. (Springer, New York, 2006).

[31] Gh.-S. Paraoanu, Phys. Rev. A **67**, 023607 (2003).

[32] S. Burger, K. Bongs, S. Dettmer, W. Ertmer, K. Sengstock, A. Sanpera, G. V. Shlyapnikov, and M. Lewenstein, Phys. Rev. Lett. **83**, 5198 (1999).

[33] J. Denschlag, J. E. Simsarian, D. L. Feder, C. W. Clark, L. A. Collins, J. Cubizolles, L. Deng, E. W. Hagley, K. Helmerson, W. P. Reinhardt, S. L. Rolston, B. I. Schneider, and W. D. Phillips, Science **287**, 97 (2000).

[34] A. Kumar, R. Dubessy, T. Badr, C. De Rossi, Mathieu de Goër de Herve, L. Longchambon, and H. Perrin, Phys. Rev. A **97**, 043615 (2018).